Journal of the Meteorological Society of Japan, Vol. 90, No. 5, pp. 629–646, 2012
DOI: 10.2151/jmsj.2012-504

Analysis of Cloud Properties Associated with Tropical Convection in Climate Models and Satellite Data

Hiroki ICHIKAWA

Department of Earth and Environmental Sciences, Graduate School of Environmental Studies, Nagoya University, Nagoya, Japan

Hirohiko MASUNAGA

Hydrospheric Atmospheric Research Center, Nagoya University, Nagoya, Japan

Yoko TSUSHIMA

Met Office Hadley Centre, United Kingdom

and

Hiroshi KANZAWA

Department of Earth and Environmental Sciences, Graduate School of Environmental Studies, Nagoya University, Nagoya, Japan

(Manuscript received 2 April 2012, in final form 3 July 2012)

Abstract

Cloud properties associated with tropical convection are analyzed for 11 models participating in Cloud Feedback Model Intercomparison Project Phase 1 (CFMIP1) in comparison with International Satellite Cloud Climatology Project (ISCCP) and other satellite observations and reanalysis datasets. Cloud properties are analyzed for different regimes of large-scale circulation field sorted by monthly mean of pressure coordinated vertical velocity at 500 hPa as an index of large-scale circulation. The present analysis is focused on warm oceanic regions with sea surface temperatures above 27°C where convection is active. The warm oceanic regions cover the vertical motion regimes ranging from strong ascent to weak descent. The ISCCP simulator outputs are used to evaluate cloud properties in the models. Cloud amount of optically thick high-clouds with optical thicknesses (τ) $\geqq$ 3.6 and cloud-top pressure (CTP) $\leqq$ 440 hPa is overestimated in the strong ascent regime while that of optically thin high-clouds with τ < 3.6 is underestimated for all the regimes. Cloud amount of optically thick low-clouds with CTP $\geqq$ 680 hPa is overestimated in the weak vertical motion regime as well in some models. The relevance of cloud amount bias to cloud radiative effect bias is discussed.

Observations show that optically thick clouds in the strong ascent regime often have tops around 180–310 hPa. In many models, the cloud top often reaches higher altitude compared to the observations. The tendency can especially be seen in the models adopting the moisture accumulation type scheme presumably due to excessively deep convection. Comparison of upward motion strength among the models and reanalyses suggests that cumulus parameterization performs better when entrainment rate is varied with large-scale environmental fields to reduce the convection deepness where necessary.

Corresponding author: Hiroki Ichikawa, Okada Patent Service Co. Ltd., 7th floor of Nagoya Chamber of Commerce & Industry Building, 10-19, Sakae 2-chome, Naka-ku, Nagoya 460-0008, Japan
E-mail: ichikawahtrr@gmail.com

1. Introduction

This study mainly analyzes clouds associated with convective activity over oceanic regions in the tropics (30S-30N). Clouds of this type as well as those of other

types play an important role in regulating radiative balance/imbalance at the top-of-atmosphere (TOA) over the region. One of the properties of the cloud radiative effect, often called cloud radiative forcing (CRF), in association with convective activity over the region is that longwave CRF (LWCRF) and shortwave CRF (SWCRF) nearly cancel each other (Ramanathan et al. 1989; Kiehl and Ramanathan 1990; Kiehl 1994; Hartmann et al. 2001). Yuan et al. (2008) examined the effect of large-scale circulation field on the relationship of LWCRF and SWCRF over the region with high sea surface temperatures (SSTs), and showed that the near cancellation between the two CRFs occurs irrespectively of different large-scale circulation regimes sorted by pressure-coordinated vertical motion at 500 hPa (ω500).

The response of CRF associated with convective activity in the tropics to an imposed climate perturbation in model experiments shows no consistency in either sign or magnitude among different climate models (Bony et al. 2004; Wyant et al. 2006; Williams and Tselioudis 2007; Williams and Webb 2009). A detailed analysis of model physics for clouds associated with convective activity is warranted to obtain physical insights on what gives rise to the differences in the CRF response. The analysis may involve model evaluation and unraveling model bias as was done in several studies (e.g., Su et al. 2006; Ichikawa et al. 2009; Waliser et al. 2009; Williams and Webb. 2009). Ichikawa et al. (2012), hereafter IMTK12, evaluated the relationship between LWCRF and SWCRF over warm oceanic regions with SSTs above 27°C in the tropics for different ω500 regimes in coupled atmosphere-ocean general circulation models (AOGCMs) participating in Coupled Model Intercomparison Project Phase 3 (CMIP3). They revealed that the ratio of LWCRF to SWCRF in the models is close to the observed ratio in the strong ascent regime, but is systematically underestimated in the weak vertical motion regime. In IMTK12, however, cloud properties responsible for the CRF bias were not investigated in depth.

The International Satellite Cloud Climatology Project (ISCCP) simulator (Klein and Jokob 1999; Webb et al. 2001), which mimics the ISCCP cloud classification, is one of the major tools to evaluate each model's cloud properties. It classifies model's clouds into several types based on the optical thickness (τ) and cloud-top pressure (CTP) using the model's radiation routine. Several studies evaluated cloud amount for different types of model clouds using the ISCCP simulator (e.g., Lin and Zhang 2004; Ringer and Allan 2004; Zhang et al. 2005; Wyant et al. 2006; Williams and Tselioudis 2007; Williams and Webb 2009). Wyant et al. (2006) analyzed the simulated cloud properties for different ω500 regimes in the tropical land and ocean. They showed that models tend to make the mistake of giving optically thick clouds over the region where satellites of ISCCP observe optically thin clouds.

This study evaluates cloud properties associated with convective activity in the models participating in Cloud Feedback Model Intercomparison Project (CFMIP, McAvaney and Le Treut 2003; http://www.cfmip.net) which provides the ISCCP simulator outputs. The result of IMTK12 motivates us to conduct an analysis of the cloud properties. While IMTK12 analyzed the twentieth-century simulations conducted by coupled AOGCMs, this study analyzes the equilibrium control experiment conducted by coupled atmosphere-mixed layer slab ocean models. Because ocean heat transport in the equilibrium control experiment is prescribed in order to maintain a seasonal cycle of SSTs which is as close as possible to the observed climatology, any model bias that appears in the current analysis may be ascribed mainly to an intrinsic bias of the atmospheric general circulation model (AGCM). Thus, this study can reveal a model bias of cloud properties mainly caused by the AGCM component, not largely contaminated by the biases caused by the oceanic general circulation model (OGCM) component and coupling between the AGCM and the OGCM.

Following IMTK12, this study focuses on warm oceanic regions with SST above 27°C in the tropics. Cloud properties are evaluated for different regimes using ω500 as an index of large-scale circulation. First, the model reproducibility of CRF is analyzed in the same way as IMTK12. Next, the model reproducibility of cloud amount for different cloud types is analyzed. Finally, how the model reproducibility of cloud amount for different cloud types affects that of CRF is discussed. This study employs a wide range of models with different types of cumulus parameterization schemes to facilitate a systematic intercomparison of the parameterization schemes among the models. Such an intercomparison may provide useful information to improve model physics.

Section 2 outlines the observational and reanalysis data and model simulations used in this study. Section 3 describes the method for the present analysis. Section 4 presents the results of the reproducibility of CRF and cloud amount associated with convective activity in the models. Section 5 is devoted to a discussion on the result. Section 6 presents conclusions of this study.

2. Data

Following IMTK12, all the data used in this study are interpolated to the common 2.5° × 2.5° grid in horizontal, the same coordinate system as reanalysis datasets, using the method by Kosaka et al. (2009).

2.1 Observational and reanalysis data

Three observational and reanalysis datasets used in this study are the same as used in IMTK12. The Earth Radiation Budget Experiment (ERBE) S-9 data (Barkstrom1984; Barkstrom and Smith 1986) are used to calculate CRF. The 40-year European Centre for Medium-Range Weather Forecasts (ECMWF) Re-Analysis (ERA-40) data (Uppala et al. 2005) are used for atmospheric fields. The Hadley Centre Global Sea Ice and Sea Surface Temperature (HadISST) analyses (Rayner et al. 2003) are used for SST.

The followings are observational and reanalysis datasets used in this study but not in IMTK12. The ISCCP D1 VIS/IR cloud data (Rossow and Schiffer 1999) are used for cloud amount in this study instead of ISCCP D2 cloud data used in IMTK12. This is because cloud amount is provided for finer τ-CTP categories in the ISCCP D1 data than in the ISCCP D2 data. The ISCCP D1 data provide cloud amount in six categories of τ partitioned by 1.3, 3.6, 9.4, 23, and 60 and in seven categories of CTP partitioned by 800, 680, 560 440, 310, and 180 hPa at every 3 hour for day-light hours only, while the ISCCP D2 data provide cloud amount in three categories of τ partitioned by 3.6 and 23 and in three categories of CTP partitioned by 680 and 440 hPa on a monthly mean basis. Considering potential differences in atmospheric fields among reanalysis datasets, ECMWF Interim reanalysis (ERA-Interim; Dee et al. 2011) and Japanese 25-yr reanalysis (JRA-25; Onogi et al. 2007) data are used in this study as well as ERA-40 data.

Monthly averages for 5 years and 1 month of February 1985 – February 1990 of the above datasets are mainly used for the analysis. The period of the analysis is limited by the observational period of ERBE.

In addition, following datasets based on satellite observation are used to discuss the result of analysis. For the vertical profile of cloud amount, the monthly mean product of CloudSat Reflectivity Data (available in CFMIP website: http://climserv.ipsl.polytechnique.fr/cfmip-obs/) which is generated from the Level 2 GEOPROF product (Mace et al. 2008; Marchand et al. 2008) is used. The data contain reflectivity-height histograms with the dBZ values binned by 5 dBZ intervals in the range of –50 dBZ to 25 dBZ and the altitude binned by 480m intervals from surface to 20 km in height. For humidity field in the lower and upper troposphere, *Aqua* Atmospheric Infrared Sounder (AIRS)/ Advanced Microwave Sounder Unit (AMSU) version 5 level-3 monthly product (Olsen et al. 2007) is used. In addition, for humidity field in the upper troposphere, *Aura* Microwave Lim Sounder (MLS) version 3.3 level-3 monthly product (Livesey et al. 2011) which is prepared for the comparison with GCM outputs (available at ftp://mls.jpl.nasa.gov/pub/outgoing/fullerr/cmip/) is used. Monthly averages for 4 years and 7 month of June 2006 – December 2010 of the above datasets are used. The period of the analysis is set to the period available for CloudSat data.

2.2 Climate models

a. Overview

This study uses outputs from the equilibrium control experiments conducted by 11 coupled atmosphere-mixed layer slab ocean models (Table 1). Fully coupled model versions of the models (AOGCMs) are participating in CMIP3, except CCCMA4.0, HadSM4, and UIUC. Three of the Met Office Hadley Centre models are included in our study. HadGSM1 and HadSM3 have considerable structural differences from each other, including different dynamical cores, spatial resolutions, and physical parameterizations. HadSM4 is different from HadSM3 with respect to physical parameterizations and vertical resolution. Two versions of MIROC3.2 with different climate sensitivities are included in our study. The higher and lower sensitivity versions of the model are referred as ''MIROC-s-hi'' and ''MIROC-s-lo'', respectively. More information of all the models analyzed in this study can be found in Webb et al. (2006) and Williams and Webb (2009).

ISCCP simulator outputs are included in CFMIP model outputs. ISCCP simulator outputs provide cloud amount in seven categories of τ partitioned by 0.3, 1.3, 3.6, 9.4, 23, and 60 and seven categories of CTP partitioned in the same way as the ISCCP observations. The data are available for day-light hours only. The ISCCP simulator output has one additional category of $\tau < 0.3$, which is below the least detectable limit of τ in the ISCCP product. This study evaluates clouds with $\tau > 0.3$ in the models. However, the choice of the threshold value of 0.3 is somewhat arbitrary (Zhang et al. 2005). Thus, careful interpretation is needed for discussing the difference of optically thin clouds between the ISCCP simulator output and the ISCCP observations.

Monthly mean outputs for 5 years are analyzed for each model except ECHAM5 and MIROC-s-hi where monthly outputs are unavailable. Five years is the

Table 1. Description of 11 models analyzed in this study. 'T' and 'N' in the column of resolution means the truncation of spectral models and half the number of east–west points for grid-point models, respectively. 'L' in the column means the number of vertical atmospheric levels.

Modeling group	Model name	Resolution (Horizontal/ Vertical)	Main references	Cumulus parameterization scheme/Label in this paper	Modification of cumulus parameterization scheme
Canadian Centre for Climate Modeling and Analysis	CCCMA4.0	T47/L35	von Salzen et al. (2005)	Zhang and McFarlane (1995)/ZM	
National Center for Atmospheric Research	CCSM3	T85/L26	Collins et al. (2006)	Zhang and McFarlane (1995)/ZM	
Max Planck Institute for Meteorology	ECHAM5	T63/L31	Roeckner et al. (2003)	Tiedtke (1989)/MC	Nordeng (1994)
NOAA/Geophysical Fluid Dynamics Laboratory	GFDL2.1	N72/L24	Delworth et al (2006)	Moorthi and Suarez (1992)/AS	Tokioka et al. (1988)
Hadley Centre for Climate Prediction and Research/ Met Office	HadGSM1	N96/L38	Martin et al. (2006)	Gregory and Rowntree (1990)/CBB	
Hadley Centre for Climate Prediction and Research/ Met Office	HadSM3	N48/L19	Pope et al. (2003)	Gregory and Rowntree (1990)/CBB	
Hadley Centre for Climate Prediction and Research/ Met Office	HadSM4	N48/L38	Webb et al. (2001)	Gregory and Rowntree (1990)/CBB	
Meteo-France/Centre National de Recherches Meteorologiques	IPSL4	N48/L19	Hourdin et al. (2006)	Emanuel (1991)/EM	Grandpeix et al. (2004)
Center for Climate System Research, National Institute for Environmental studies, and Frontier Research Center for Global Change	MIROC-s-hi (MIROC3.2)	T42/L20	K-1 Model Developers (2004)	Pan and Randall (1998)/ AS	Emori et al. (2001)
Same as above	MIROC-s-lo (MIROC3.2)	T42/L20	K-1 Model Developers (2004)	Pan and Randall (1998)/ AS	Emori et al. (2001)
Climate Research Group of the University of Illinois at Urbana-Champaign	UIUC	N36/L24	Yang et al. (2000)	Yang et al. (2000)/CBB	

longest period where monthly outputs are available for all models. Monthly mean data are constructed from 5 years of daily mean data for ECHAM5 and 2 years of daily mean data for MIROC-s-hi.

b. Cumulus parameterization schemes

Subgrid-scale cloudiness associated with tropical convection is largely controlled by the cumulus parameterization scheme adopted in each model. Several types of schemes are used as described in Table 1. This study classifies cumulus parameterization schemes into 5 of the 6 types in IMTK12. The Betts (1986) convective adjustment scheme is not represented in CFMIP and thus is not analyzed in this study. The remaining 5 types of scheme analyzed in this study are briefly described as follows.

Three models (GFDL2.1, MIROC-s-hi, MIROC-s-lo) adopt a scheme based on a mass flux approach with spectral cloud models similar to Arakawa and Schubert (1974). This type of scheme is hereafter named AS. The triggering mechanism and closure assumption for convection activity (hereafter referred to as convective trigger/closure) of this scheme are linked to convective available potential energy (CAPE). The modification proposed by Tokioka et al. (1988) and Emori et al. (2001), both of which set a threshold for convection occurrence, acts to relate the accumulation of moisture to convection occurrence in model simulations.

Four models adopt a scheme based on a mass flux approach with a bulk cloud model. For three models (HadgSM1, HadSM3, HadSM4, UIUC), the convective trigger/closure is based on cloud-base buoyancy proposed by Gregory and Rowntree (1990) or Yang et al. (2000). This type of scheme is hereafter named CBB. While the details of the parameterizations are significantly different between Gregory and Rowntree (1990) and Yang et al. (2000), convection in both of the two schemes depends on the stability of atmosphere. For one model (ECHAM5), the convective trigger/closure is based on moisture convergence originally proposed by Kuo (1965). This scheme is hereafter named MC.

Two models (CCCMA4.0, CCSM3) adopt the scheme proposed by Zhang and McFarlane (1995) which is based on the spectral rising plume concept as in the AS scheme but assumes a constant spectral distribution in cloud-base mass flux. The scheme is hereafter named ZM. The convective trigger/closure of this scheme links basically to CAPE. This scheme is primarily designed for deep rather than shallow cumulus convection by applying an assigned minimum depth of convection.

A model (IPSL4) adopts the scheme proposed by Emanuel (1991) which is based on a buoyancy sorting approach. This scheme is hereafter named EM. The convective trigger/closure of this scheme links basically to convective available potential energy (CAPE). The modification proposed by Grandpeix et al. (2004) acts to suppress deep convection when the free troposphere is dry in model simulations.

3. Method

3.1 Calculation of cloud radiative forcing

Following IMTK12, LWCRF, SWCRF, NetCRF (LWCRF plus SWCRF), and R (the ratio of LWCRF to SWCRF) are calculated as

$$\mathrm{LWCRF} \equiv \mathrm{OLR}_{\mathrm{clr}} - \mathrm{OLR},$$
$$\mathrm{SWCRF} \equiv \mathrm{TRS}_{\mathrm{clr}} - \mathrm{TRS},$$
$$\mathrm{NetCRF} \equiv \mathrm{LWCRF} + \mathrm{SWCRF},$$
$$\mathrm{R} \equiv -\frac{\mathrm{LWCRF}}{\mathrm{SWCRF}}$$

where OLR and TRS refer to the outgoing longwave radiation and the total reflected solar radiation, respectively, at the TOA for all-sky conditions. $\mathrm{OLR}_{\mathrm{clr}}$ and $\mathrm{TRS}_{\mathrm{clr}}$ refer to those for clear-sky conditions. CRF for different ω500 regimes is calculated on a monthly mean basis. R is calculated from the climatologies of LWCRF and SWCRF calculated with the full period analyzed in this study for each ω500 regime.

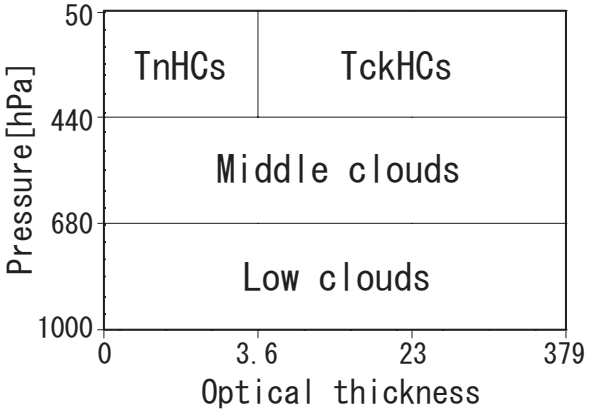

Fig. 1. Definition of cloud types in this study.

3.2 Definition of cloud types

This study compares cloud amount for different cloud types in ISCCP simulator outputs with that in the ISCCP observations. While the ISCCP simulator is a valuable tool for evaluating model reproducibility of cloudiness, definitions of τ and CTP in the ISCCP simulator are not exactly consistent with those in the ISCCP observation (Mace et al. 2011). This point should be kept in mind through this study. Nevertheless, the analysis of cloud amount for different cloud types in conjunction with that of CRF reflecting cloud properties could be quite helpful to unraveling intrinsic model biases.

This study evaluates cloud amount for 4 cloud types (Fig. 1). At first, clouds are categorized into 3 cloud types of high, middle, and low clouds. The definitions of the 3 cloud types are based on the ISCCP classification where detected CTP is smaller than 440 hPa for high clouds, between 680 hPa and 440 hPa for middle clouds, and larger than 680 hPa for low clouds. The evaluation of cloud amounts in this study is particularly focused on high clouds, which largely control CRF over the warm oceanic regions in the tropics (e.g., Yuan et al. 2008). High clouds are subdivided into optically thick high-clouds (TckHCs) with $\tau \geqq 3.6$ and optically thin high-clouds (TnHCs) with $\tau < 3.6$. In the ISCCP classification, TckHCs include deep convective clouds and cirrostratus clouds while TnHCs correspond to cirrus clouds (Rossow and Schiffer 1999). High clouds are subdivided because of the following two points. The first point is a difference in physical mechanism for cloud formation. In the observations, the occurrence of cirrus clouds does not always coincide with that of deep convective clouds and cirrostratus clouds,

while the occurrence of deep convective clouds and cirrostratus clouds are closely related with each other (e.g., Luo and Rossow 2004; Del Genio et al. 2005). The second point is a difference in CRF. Cirrus clouds act to primarily warm the atmosphere-surface system while other high clouds act to cool it (e.g., Hartmann et al. 2001; Kubar et al. 2007). When the impact of model reproducibility of cloudiness on that of CRF is discussed as will be done in section 5b, this subdivision is quite useful to identify the linkage of cloud biases with CRF biases.

4. Results

4.1 Reproducibility of ω500

First of all, the model reproducibility of ω500 is analyzed. As an important aspect, Fig. 2 shows the probability density function (PDF) of ω500 in domains of warm SSTs above 27°C for reanalysis datasets and the models. The model-line colors are based on cumulus parameterization scheme. Following IMTK12, this study defines 4 regimes as shown in Table 2. In reanalysis datasets, the PDF exhibits a moderate peak in the weak vertical motion regime, declining gradually toward stronger ascending motion and sharply toward stronger descending motion. In most models, the PDFs agree overall with those in reanalysis datasets. Close examination reveals the differences of PDF reproducibility among models. In IPSL4, the PDF peak biases leftward against the reanalysis datasets, while the PDF width is reasonable. In UIUC, the PDF width is narrower than the reanalysis datasets while the PDF peak is roughly reasonable.

4.2 Reproducibility of CRF

This subsection evaluates CRF over the warm oceanic regions. Overall features of model reproducibility of CRF described below are generally similar to those in IMTK12. Figure 3 shows the composite of (a) LWCRF, (b) SWCRF, (c) NetCRF, and (d) R as a function of ω500. The absolute value of CRF is hereafter referred to as the CRF magnitude. The models agree qualitatively well with the ERBE observations in the relationships of LWCRF and SWCRF with ω500: the two CRFs vary almost linearly with ω500 in the models as do in the ERBE observations. LWCRF and SWCRF in the models spread around the ERBE observations over a range of ~40 W m^{-2} at each ω500.

The magnitude of inter-model spread of NetCRF is similar to that of each LWCRF and SWCRF. NetCRFs of the models are generally overestimated in magnitude. Rs in the models are relatively close to the ERBE observations in the strong ascent regime. The reasonable R results from LWCRF and SWCRF in some models (e.g., ECHAM5, GFDL2.1, HadGSM1), while it occurs as a result of the compensation of overestimated LWCRF and SWCRF in magnitude in some models (e.g., CCSM3, HadSM4, IPSL4, MIROC-s-lo). The model reproducibility of R worsens with increasing ω500 for all models. In the weak vertical motion regime, R is systematically underestimated in most models. This underestimation of R is associated mainly with the underestimation of LWCRF in most models, and is also associated with the overestimation of SWCRF in magnitude in some models (e.g., CCSM3, MIROC-s-hi, MIROC-s-lo).

4.3 Reproducibility of cloud amount

This subsection evaluates cloud amount for different cloud types. In the previous subsection, it is shown that some models well reproduce CRF as a function of ω500 (Fig. 3). However, because CRF is determined from the cumulative effect of clouds having a variety of optical depths and cloud heights, high reproducibility of CRF in a model does not necessarily result from the high reproducibility of individual clouds in the model. Analyzing simulated clouds for different optical depths and CTPs is thus important to fully evaluate model physics. The following analyses are particularly focused on high clouds which largely control total CRF over the warm oceanic regions (Yuan et al. 2008).

a. Overall features

Figure 4 shows cloud amount for the 4 cloud types for the ISCCP observations and the models as a function of ω500. Most models qualitatively agree well with the ISCCP observations in the relationships of TckHC amount and TnHC amount with ω500: both cloud types' values decrease with increasing ω500. However, for TckHC amount, the gradient is steeper in the models than in the ISCCP observations. Most of the models overestimate TckHC amount in the strong ascent regime. TnHC amount is underestimated for all the regimes in most models. However, this underestimation might be due to the cutoff value of τ at 0.3 in the ISCCP simulator outputs. When clouds with $\tau < 0.3$ are included in TnHCs in the models, TnHC amount is close to the ISCCP observations or even overestimated. Middle and low cloud amounts (Figs. 4c and d) are underestimated in most models. The underestimation of these cloud amount remains even if clouds with $\tau < 0.3$ are included in the model outputs. As shown in the next subsection, while the total low cloud amount is underestimated in the models, optically thick

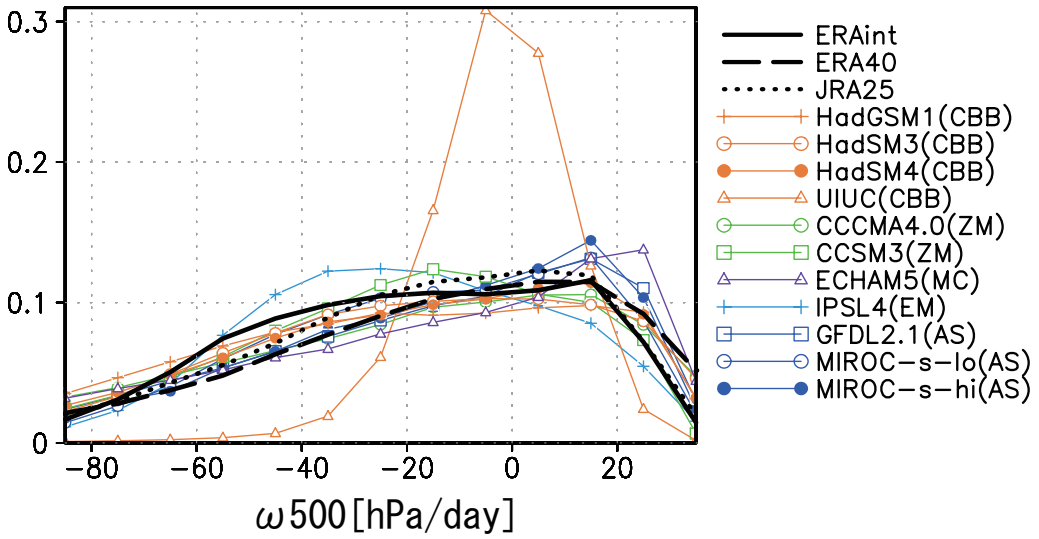

Fig. 2. PDF of ω500 for each bin of width 10 hPa day^{-1} for reanalysis data (black lines) and 11 models (color lines). The model-line colors are based on cumulus parameterization scheme which is denoted in parentheses.

Table 2. Definition of ω500 regimes in this study [hPa day^{-1}].

Strong ascent	Moderate ascent	Weak vertical motion	Moderate-strong descent
$\omega500 < -40$	$-40 < \omega500 < -10$	$-10 < \omega500 < 20$	$\omega500 > 20$

low-cloud amount is overestimated in some models.

b. Vertical distribution

In order to examine the model biases in further depth, cloud amount for the 7 vertical layers is analyzed. Analysis is particularly focused on optically thick clouds to examine the detail of overestimation of TckHC amount in the models. Pressure levels between 440–180 hPa and between 180–50 hPa are hereafter referred to as "the upper tropopshere" and "near the tropopause" respectively, for the analyses of high clouds.

Figure 5 shows the vertical distribution of cloud amount for optically thick clouds with $\tau \geqq 3.6$, including TckHCs, as a function of $\omega500$. In the ISCCP observations, the cloud amount is largest at 310–180 hPa in the strong and moderate ascent regimes. The model performance of reproducing cloudiness varies among models. At pressure below 440 hPa, the cloud amount is largest at 310–180 hPa in many models as is in the ISCCP observations. The cloud amount in the upper troposphere in nearly half of the models is roughly close to that in the ISCCP observations. On the other hand, the cloud amount near the tropopause is overestimated in the strong ascent regime in many models. This overestimation seems to cause the overestimation of TckHC amount in Fig. 4a. Models adopting cumulus parameterization schemes sensitive to moisture accumulation (ECHAM5, GFDL2.1, IPSL4, MIROC-s-hi, MIROC-s-lo) tend to overestimate the cloud amount near the tropopause. For reference, cloud amount at pressures above 800 hPa (part of low clouds) are evidently overestimated in some models (e.g., CCCMA4.0, CCSM3, MIROC-s-hi, MIROC-s-lo, UIUC).

5. Discussion

5.1 Potential relevance of model bias in cloudiness with cumulus parameterization schemes

In Section 4, near-tropopause thick cloud amount were found to be overestimated in many models compared to the ISCCP observations. However, as pointed out by Mace et al. (2011), the difference between ISCCP simulator outputs and the ISCCP observations may partly come from the retrieval error in the ISCCP observations. In order to confirm the result of the ISCCP observations, the CloudSat observations are further analyzed. Figure 6 shows the vertical distribution of cloud amount observed by the CloudSat radar as a function $\omega500$. Because the sensitivity of the

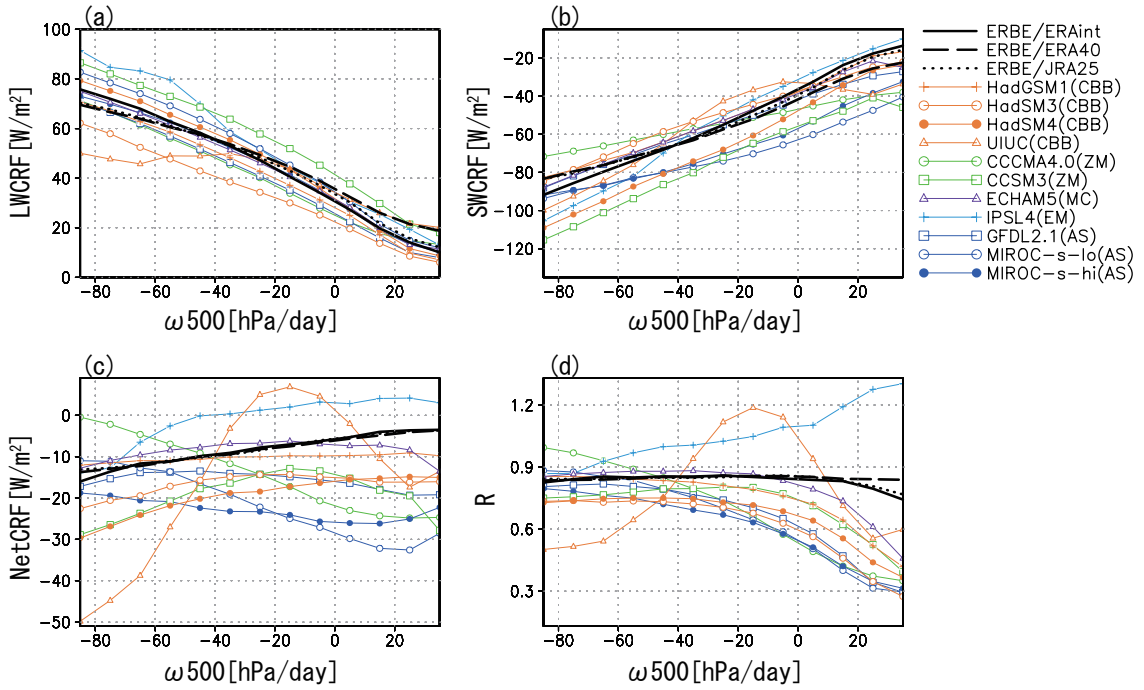

Fig. 3. Composite of (a) LWCRF, (b) SWCRF, (c) NetCRF, and (d) R as a function of ω500 for ERBE observations sorted by ω500 of reanalyses (black lines) and 11 models (color lines).

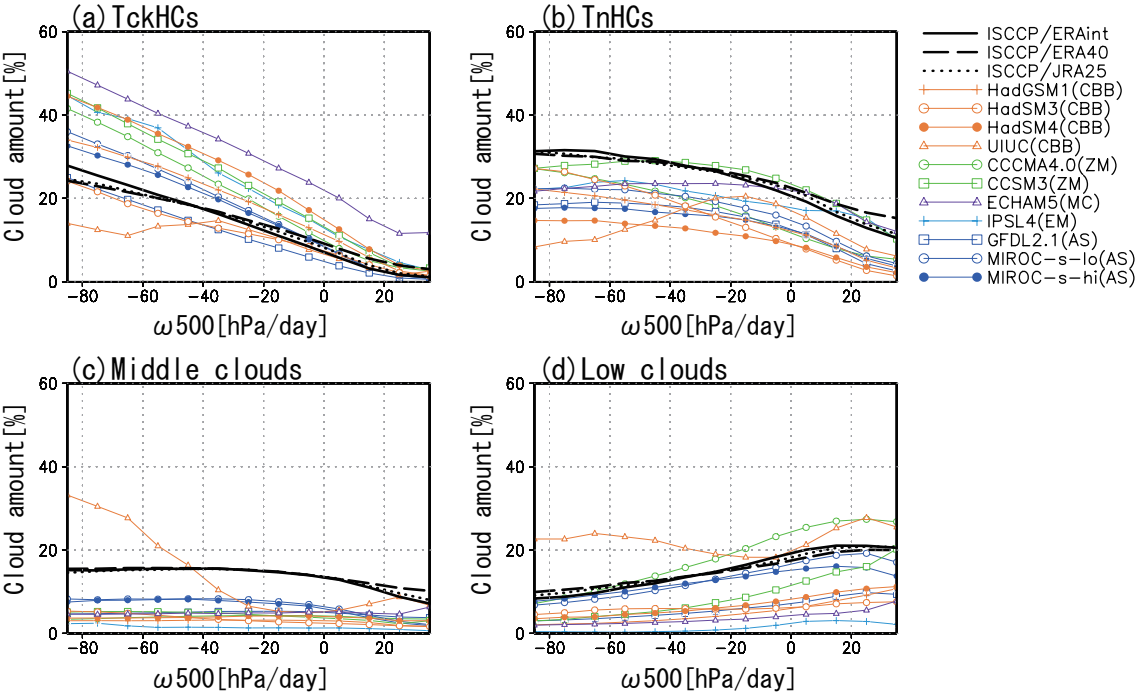

Fig. 4. Composite of (a) TckHC, (b) TnHC, (c) middle cloud, and (d) low cloud amount as a function of ω500 for ISCCP observations sorted by ω500 of reanalyses (black lines) and 11 models (color lines).

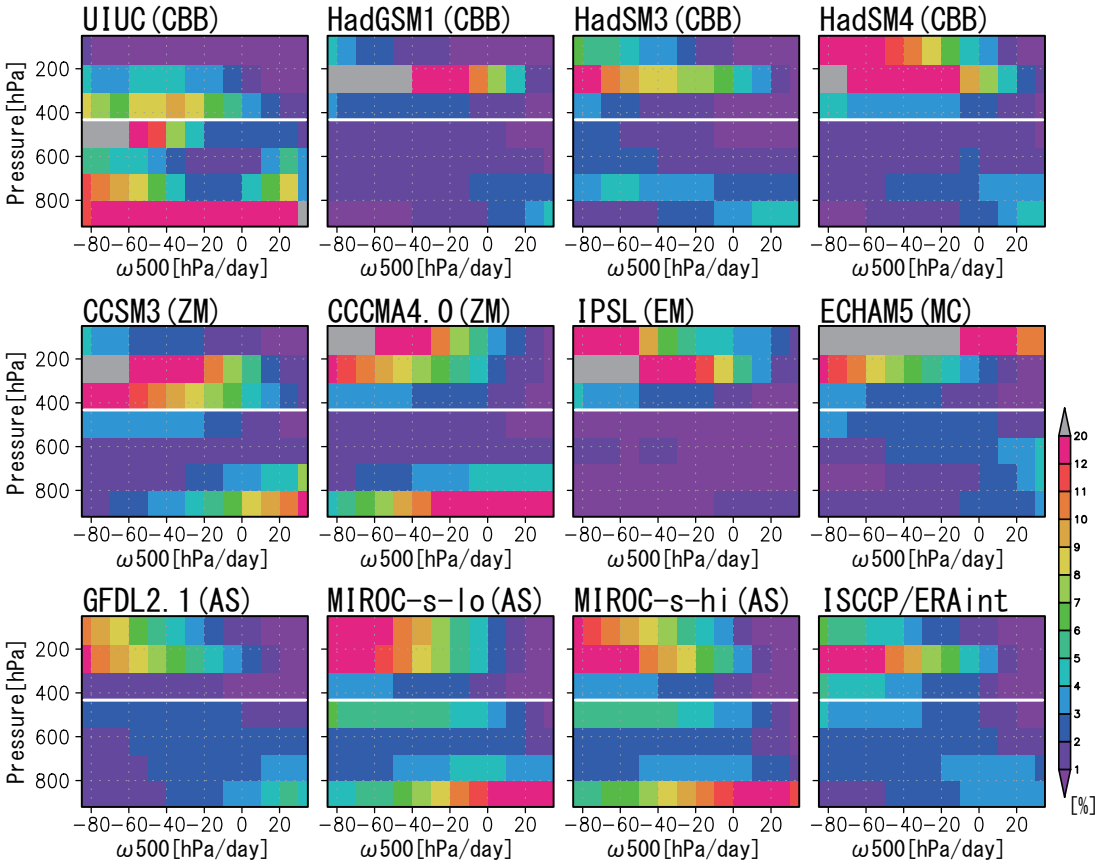

Fig. 5. Composite of cloud amount for clouds with $\tau \geqq 3.6$ at each pressure level defined by ISCCP as a function of $\omega 500$ for ISCCP observations sorted by $\omega 500$ of ERA-Interim and 11 models. A white solid line in each panel shows the pressure level at 440 hPa. Models are sorted by cumulus parameterization scheme which is denoted in parentheses.

radar is limited to relatively large cloud particles, the CloudSat observation is comparable mainly with optically thick clouds in the ISCCP observation although the CloudSat observation may partly include optically thin clouds. A large amount of cloudiness is seen for many pressure levels between 800 hPa and 180 hPa in the strong ascent regime. In the upper troposphere, a large amount of cloudiness extends from the strong ascent regime to descent regime. Cloud amount drastically decreases upward near the tropopause, where clouds are rarely detected. This result suggests that the cloud top of deep convection and associated anvil clouds rarely reaches above 180 hPa, supporting the results from the ISCCP observations.

The physical causes of the overestimation of the near-tropopause thick cloud amount in the models are next examined. TckHC formation is closely related to deep convection, so that vertical velocity field is

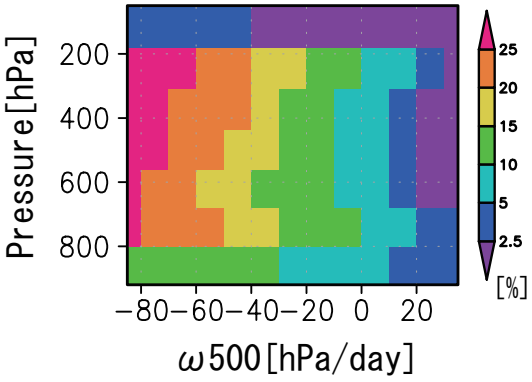

Fig. 6. Composite of vertical distribution of cloud amount as a function of $\omega 500$ for CloudSat observations sorted by $\omega 500$ of ERA-Interim. Cloud amount are estimated based on the relative frequency of occurrence for the dBZ above -25 in the CloudSat observations.

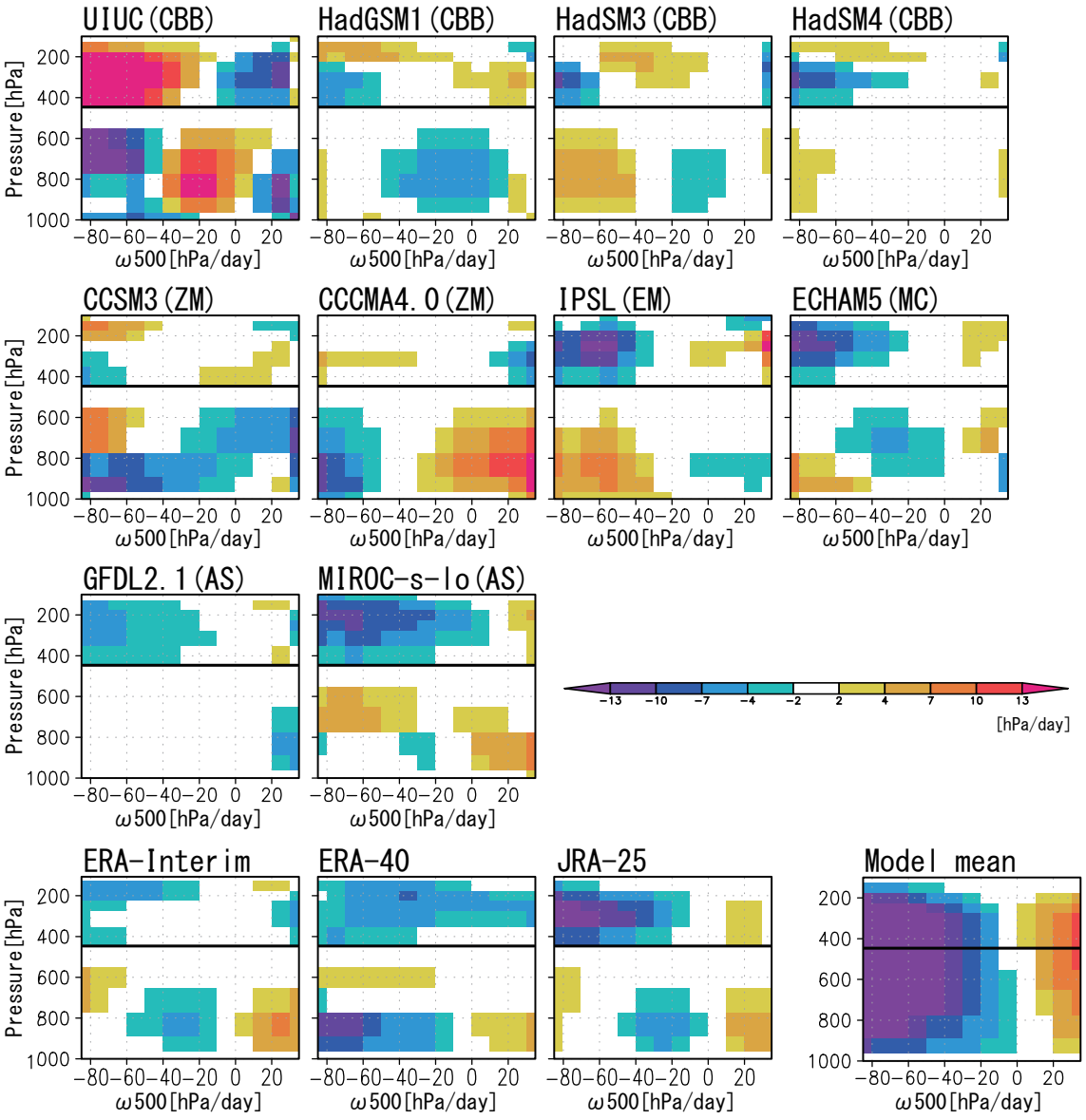

Fig. 7. Composite of vertical distribution of ω as a function of ω500 for available 10 models and 3 reanalyses. The CFMIP dataset does not provide vertical profile of ω for MIROC-s-hi. Anomaly from multi-model mean, which is displayed at right bottom corner, is shown for each model and reanalysis. For multi-model mean, multiply the values of the scale bar by 3.0. A black solid line in each panel shows the 440-hPa pressure level.

analyzed. Figure 7 shows the anomaly of vertical velocity in each model and reanalysis against the multi-model mean as a function of ω500. From now on, the pressure level at 200 hPa is included in the near tropopause category because upward motion just below 180 hPa largely affects cloud formation above that level. In the strong ascent regime, a deep layer of strong upward motion appears in the upper troposphere and near the tropopause in the many models, overestimating near-tropopause thick clouds (e.g., ECHAM5, IPSL4, GFDL2.1, MIROC-s-lo).

In order to examine the relationship of near-tropopause thick cloud amount and upward motion strength, Fig. 8 shows a scatter plot between the two parameters in the strong ascent regime. In general, at the near tropopause, a model with stronger upward

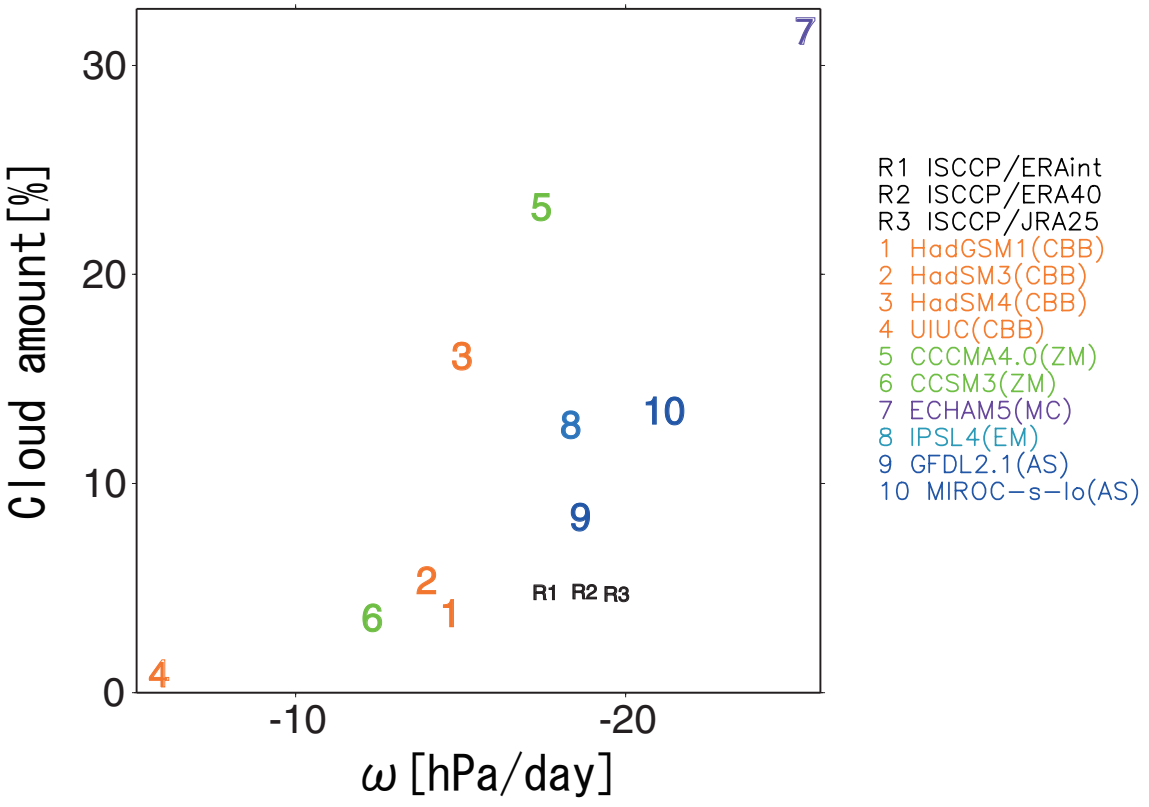

Fig. 8. Scatter plots of near-tropopause thick cloud amount against ω in the strong ascent regime for available 10 models. Plots of ISCCP observations against reanalyses are also shown. Near-tropopause ω is derived by an average of ω between 100 hPa and 200 hPa. Inter-model correlation coefficient between the two components is 0.73, which exceeds the 95 % level of significance.

motion tends to simulate larger amount of thick cloud. Close examination reveals that upward motion is stronger in GFDL2.1, IPSC4, and MIROC-s-lo than in CCCMA4.0 and HadSM4, but optically thick cloud amount is larger in the latter than in the former. Cloud formation processes appear to be linked to upward motion in different ways from one model to another.

In Fig. 8, the inter-model difference in vertical velocity field in the strong ascent regime is closely tied with the cumulus parameterization scheme adopted in each model. In general, upward motion strength is stronger in the models adopting a scheme which needs moisture accumulation for convection occurrence (i.e., AS with a threshold, modified EM, and MC) than in the models adopting the CBB and ZM type schemes. The upward motion strength of reanalyses is, on average, close to the two models adopting moisture accumulation type scheme (GFDL2.1 and IPSL4). Compared to ERA40 and JRA25, upward motion strength is reduced in ERA-interim, where a deep layer of enhanced upward motion in the upper-troposphere and near the tropopause is almost absent (Fig. 7).

In order to examine the large-scale environment for deep convection occurrence, moisture fields in the low and mid levels of troposphere are examined. Figure 9 shows relative humidity at 925 hPa and at 700 hPa as a function of ω500. Inter-model difference of relative humidity is smaller at 925 hPa than at 700 hPa. Relative humidity at 700 hPa in the strong ascent regime shows systematic differences depending on cumulus parameterization scheme adopted in each model. The relative humidity is high in the models adopting moisture accumulation type scheme (blue in Fig. 9), where near-tropopause upward motion is strong (see Figs. 7, 8). The relative humidity is moderate in the models adopting the CBB type scheme (orange in Fig. 9), but is low in the ZM scheme (green in Fig. 9). The relative humidity in the AIRS observations is lower than that in the models adopting the moisture accumulation type and the CBB type schemes. One needs to keep in mind

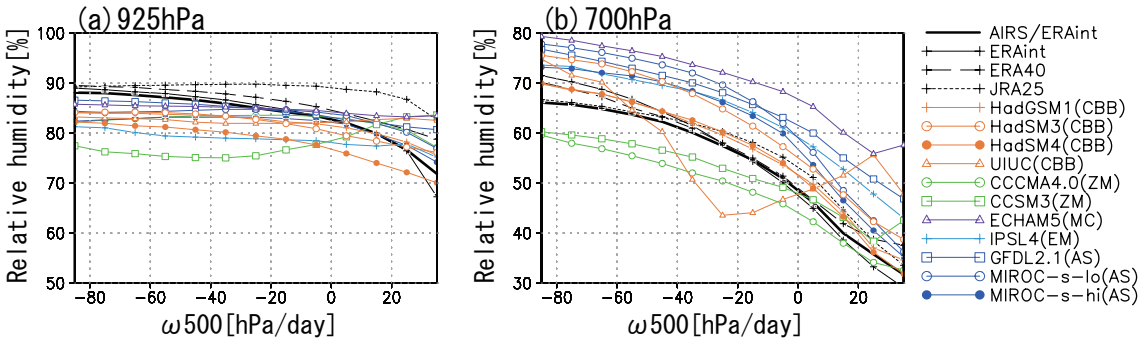

Fig. 9. Composite of relative humidity at (a) 925 hPa and (b) 700 hPa as a function of ω500 for AIRS observations sorted by ω500 of ERA-interim (a black line with no mark), reanalyses (black lines with marks), and 11 models (color lines).

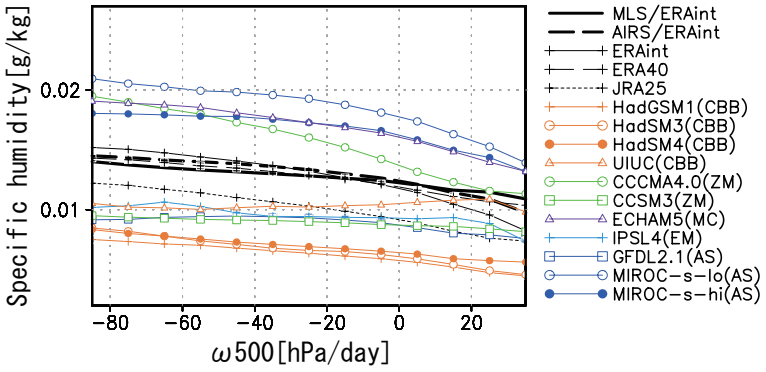

Fig. 10. Composite of specific humidity at 150 hPa as a function of ω500 for AIRS and MLS observations sorted by ω500 of ERA-interim (black lines with no mark), reanalyses (black lines with marks), and 11 models (color lines).

the fact that AIRS retrieval algorithm could be biased toward clear-sky conditions. The relative humidity in the two of the three reanalyses is higher than that in the AIRS observations (Fig. 9).

Near-tropopause thick cloud amount formation links not only to upward motion but also to moisture supply. Figure 10 shows specific humidity at 150 hPa as a function of ω500. In the strong ascent regime, the specific humidity tends to be high in the models adopting moisture accumulation type scheme (blue in Fig. 10) where near-tropopause thick cloud amount tends to be large (see Figs. 5, 8); Three out of four of the models overestimate the specific humidity compared to the observations. The specific humidity is high and overestimated also in CCCMA4.0 where the cloud amount is large (see Figs. 5, 8).

5.2 *The relevance of cloud amount bias with the CRF bias*

In this subsection, the impact of cloud amount bias on the CRF bias in the models is discussed. Figures 11 and 12 show the individual CRF for each cloud type in the ISCCP observations and the models. The method for constructing data of Figs. 11, 12 is same as used in Yuan et al. (2008). First, we calculate CRF for each of the 42 τ-CTP categories of ISCCP: we take the overcast-sky CRF values calculated by Hartmann et al. (2001), where the radiation model developed by Fu and Liou (1992, 1993) is used, for the 42 categories and then multiply the CRF values by their cloud amounts. Second, these results are aggregated to produce CRFs for 4 cloud types (TckHCs, TnHCs, middle clouds, and low clouds). Figures 11 and 12 are useful to discuss the relative contribution of each cloud type to CRF. Rela-

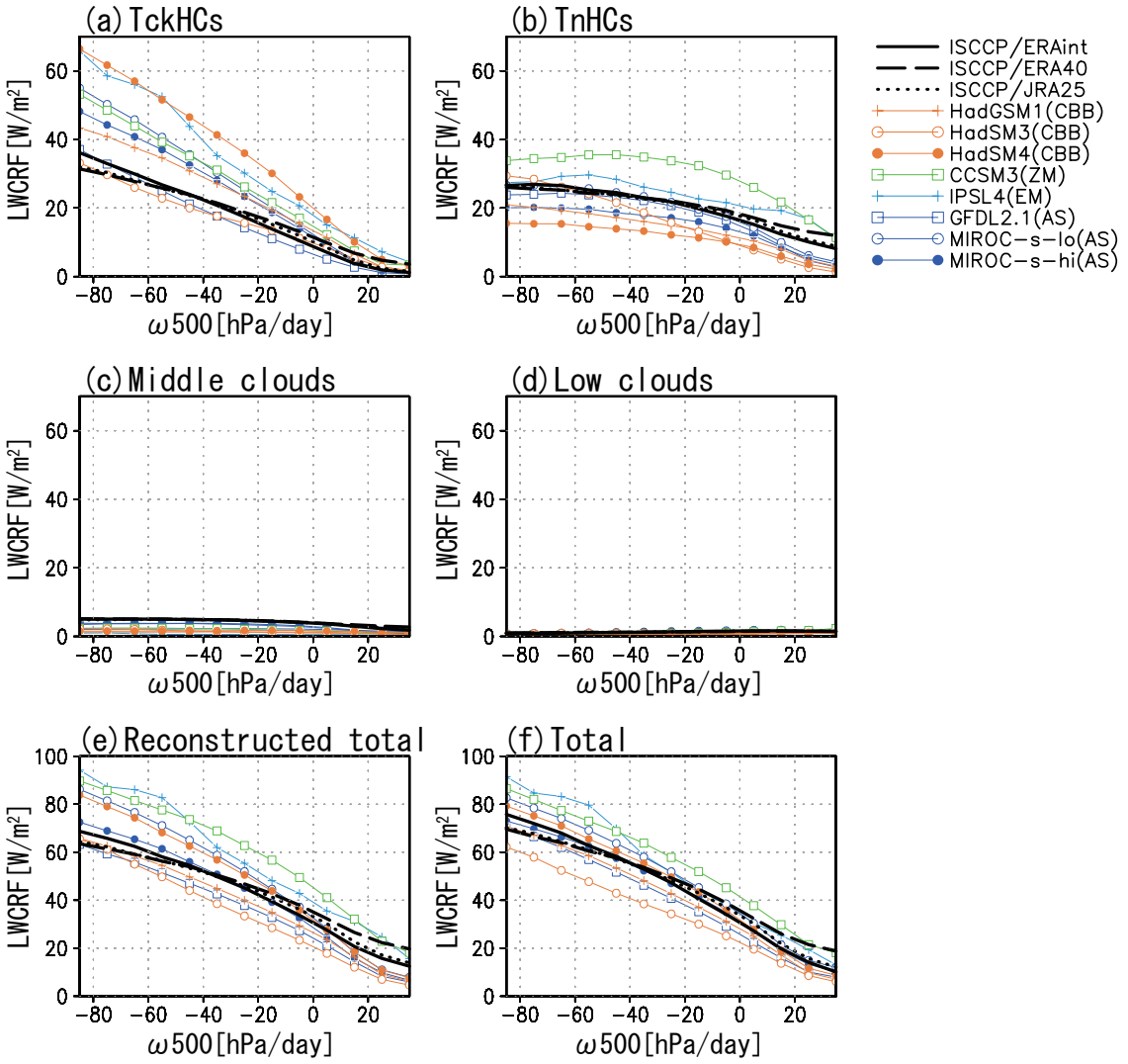

Fig. 11. LWCRF by (a) TckHCs, (b) TnHCs, (c) middle clouds, and (d) low clouds in ISCCP observations sorted by ω500 of reanalyses and 8 models (see the text for details of the calculation method). Reconstructed total LWCRF combining the effects of all 4 cloud types and total LWCRF which is identical to LWCRF in Fig. 3 are plotted in (e) and (f), respectively. Three models of CCCMA4.0, ECHAM5, and UIUC are omitted because the reconstructed CRF is far different from the total CRF.

tive differences of CRF magnitude between the observation and the models, and among models themselves in reconstructed total CRF combining the effects of all 4 cloud types (Figs. 11e, 12e), is generally consistent with those in total CRF (Figs. 11f, 12f).

Figure 11 shows the contribution of 4 cloud types to LWCRF. TckHCs and TnHCs largely control total LWCRF both in the observations and the models for all ω500s. Model biases of total LWCRF are related to those of LWCRF by individual clouds as described below. In the strong ascent regime where total LWCRF is overestimated or reasonable, LWCRF by TckHCs is overestimated in most models. This overestimation is partly compensated by the underestimation of LWCRF by TnHCs in some models (e.g., HadGSM1, HadSM4, MIROC-s-hi). In the weak vertical motion regime where total LWCRF tends to be underestimated, LWCRFs by TckHCs and TnHCs are roughly reasonable and underestimated in most models, respectively. As was described in Subsection 2.2 and Subsec-

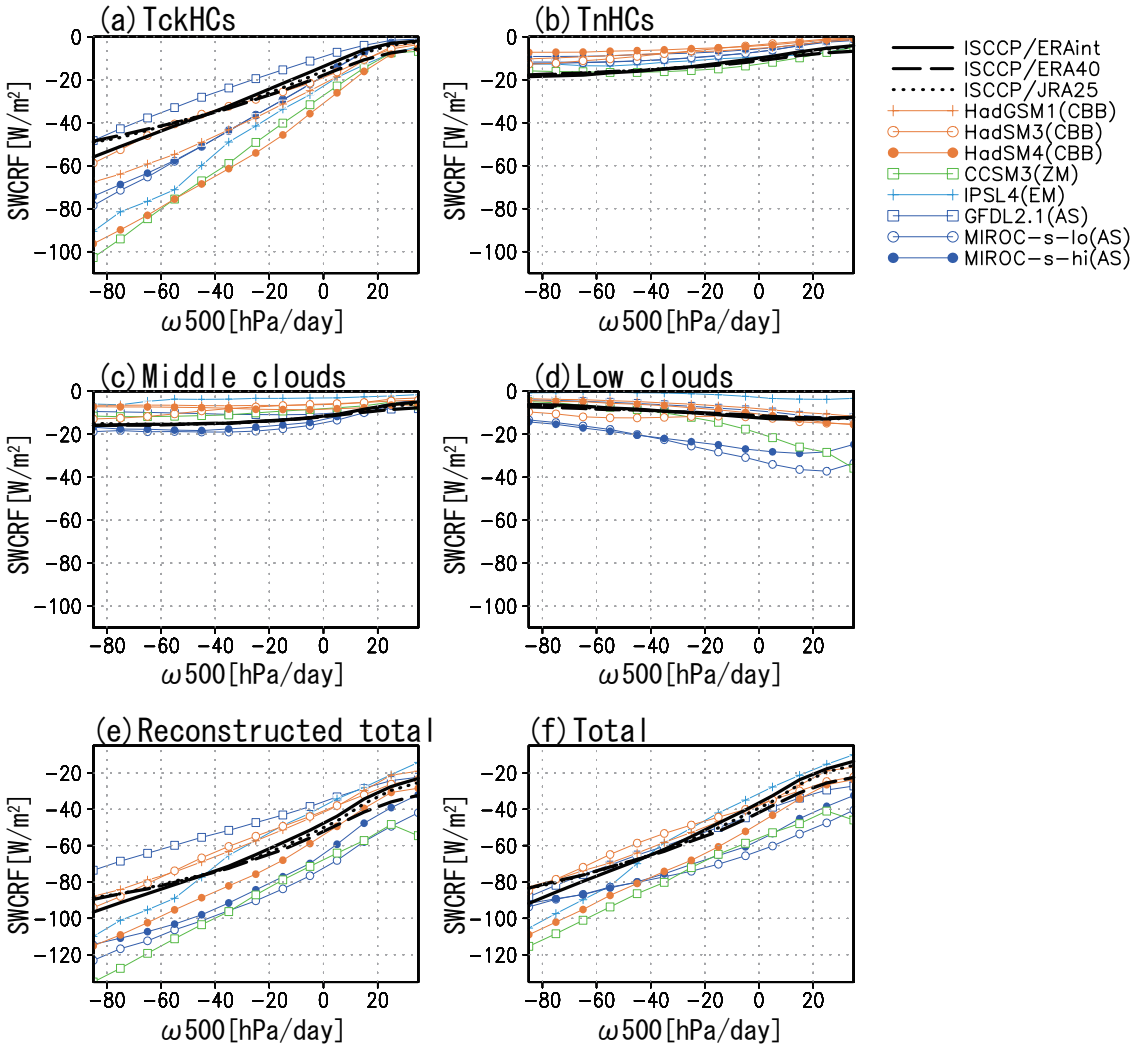

Fig. 12. Same as Fig. 11 but for SWCRF.

tion 4.3, accurate evaluation of TnHC amount is difficult in the current analysis. However, unless TnHC amount is underestimated in the models (Fig. 4b), underestimation of the total LWCRF in the weak vertical motion regime cannot be explained. Thus, it seems to be certain that radiatively effective TnHC amount is underestimated in the models.

Figure 12 shows the contribution of 4 cloud types to SWCRF. In the observations, TckHCs largely control total SWCRF in the strong ascent regime, but all 4 cloud types equally contribute to total SWCRF in the weak vertical motion regime. Model biases of total SWCRF are related to those of SWCRF magnitude by individual cloud as described below. In the strong ascent regime where total SWCRF is overestimated or reasonable, SWCRF by TckHCs is overestimated in most models. This overestimation is partly compensated by the underestimation of SWCRF by TnHCs and middle clouds. In the weak vertical motion regime where total SWCRF is overestimated in some models, SWCRF by low clouds is overestimated in those models (e.g., CCSM3, MIROC-s-hi, MIROC-s-lo). Overestimation of cloud amount with optically thick low-clouds (Fig. 5) is responsible for this bias.

6. Conclusions

The reproducibility of cloud amount and CRF associated with tropical convection over warm oceanic

regions with SSTs above 27°C is evaluated for 11 models participating in CFMIP. Cloud amount and CRF are evaluated for different regimes of large-scale circulation field sorted by ω500 as an index of large-scale vertical motion field. The warm oceanic regions cover a variety of vertical motion regimes ranging from strong ascent to weak descent.

In the warm oceanic regions, LWCRF and SWCRF nearly cancel each other irrespectively of ω500 in the ERBE observations. The absolute value of the ratio of LWCRF to SWCRF, R, is well reproduced in the models in the strong ascent regime: This is brought by reasonable LWCRF and SWCRF in some models while by the compensation of opposite overestimation biases of LWCRF and SWCRF in other models. R is systematically underestimated in the models in the weak vertical motion regime: This is associated with the underestimation of LWCRF in most models, while with the overestimation of SWCRF in some models.

In order to unravel the model biases of cloudiness responsible for the CRF biases, ISCCP simulator outputs are evaluated in comparison with the ISCCP observations. The evaluation is focused mainly on high clouds with cloud-top pressures below 440 hPa, because they have strong impacts on CRF over the warm oceanic regions. High clouds are classified into optically thick high clouds (TckHCs) with $\tau \geqq 3.6$ and thin high clouds (TnHCs) with $\tau < 3.6$. TckHC amount tends to be overestimated in the models in the strong ascent regime. TnHC amount in the models is underestimated irrespectively of ω500. However, this underestimation may be related to the arbitrary cut off value of τ at 0.3 in the ISCCP simulator outputs. Optically thick low-cloud amount is overestimated in the weak vertical motion in some models.

The ISCCP and CloudSat observations show that cloud top of optically thick clouds often appears at 310–180 hPa in the strong ascent regime. On the other hand, in many models, the cloud-top often reaches higher altitudes compared to the observations. In particular, models adopting the moisture accumulation type scheme exhibit such tendency. In general, TckHC amount increases in a model as upward motion is enhanced in the models. While the model dependence of linkage of cloud formation processes with upward motion needs to be considered, convection in these models is deeper and detrains more condensates a too high a level and tends to make more thick clouds there.

Intermodel difference in convection strength strongly depends on relative humidity in the lower free troposphere as was pointed out by previous studies (e.g., Gregory and Miller 1989, Derbyshire et al. 2004, Takayabu et al. 2010). As relative humidity in the lower free troposphere increases, convection strength increases presumably through a reduction of dry air entrainment. The importance of moisture accumulation for proper simulation of convection occurrence has been pointed out by previous studies (e.g., Tokioka et al. 1988, Emori et al. 2001, Zhang and Mu. 2005, Lin et al. 2007, Lin et al. 2008). However, in the models adopting moisture accumulation type scheme analyzed in this study, convection seems to be too deep when relative humidity is high in lower free troposphere. Difference in upward motion strength between ERA-Interim and ERA-40 may provide important insight to the convection deepness in the cumulus parameterization schemes. Upward motion strength is reduced in ERA-Interim where entrainment rate varies depending on the large-scale environmental field with no prescribed moisture accumulation (Bechtold et al. 2008), compared to ERA-40, where entrainment rate is originally imposed with prescribed moisture accumulation (Gregory et al. 2000). In the models analyzed in this study, entrainment rate is originally imposed in their cumulus parameterization schemes with prescribed moisture accumulation. The introduction of state-dependent entrainment rate may be an effective way to simulate deep convection properly in a model.

The relevance of the cloud amount biases to the CRF bias in the models is discussed. In the strong ascent regime, the overestimation of TckHC amount causes the overestimation of LWCRF and SWCRF in most models, while the underestimation of cloud amount for other cloud types leads to the reduction of CRF in some models. In the weak vertical motion regime, the underestimation of TnHC amount causes the underestimation of LWCRF in most models, while the overestimation of optically thick low clouds causes the overestimation of SWCRF in some models. It is important to study different types of clouds individually when one tries to locate the sources of CRF biases in climate models.

The method adopted in this study is a useful approach to evaluate model reproducibility of cloud amount and CRF associated with convective activity, and can be used to evaluate it in model simulations for the CMIP5. In particular, applying the same method on the CFMIP Observation Simulator Package (COSP; Bodas-Salcedo et al. 2011) outputs which are available in the CMIP5 models will unravel model biases in depth, including microphysical properties of model clouds.

Acknowledgments

The modeling groups, the PCMDI, and the WCRP's Working Group on Coupled Modeling (WGCM) made available the WCRP CFMIP multi-model dataset. Support to this dataset is provided by the Office of Science, U.S. Department of Energy. This research was supported by the Global Environment Research Fund (S-5-2) of the Ministry of the Environment, Japan, and by the "Data Integration and Analysis System (DIAS)" Fund for National Key Technology from the Ministry of Education, Culture, Sports, Science and Technology, Japan.

References

Arakawa, A., and W. H. Schubert, 1974: Interaction of a cumulus cloud ensemble with the large-scale environment, Part I. *J. Atmos. Sci.*, **31**, 674–701.

Barkstrom, B. R., 1984: The Earth Radiation Budget Experiment (ERBE). *Bull. Amer. Meteor. Soc.,* **65**, 1170–1185.

Barkstrom, B. R., and G. L. Smith, 1986: The earth radiation budget experiment: Science and implementation. *Rev. Geophys.,* **24**, 379–390.

Bechtold, P., and Coauthors, 2008: Advances in simulating atmospheric variability with ECMWF model: From synoptic to decadal time-scales. *Quart. J. Roy. Meteor. Soc.,* **134**, 1337–1351.

Betts, A. K., 1986: New convective adjustment scheme, Part. 1, Observational and theoretical basis. *Quart. J. Roy. Meteor. Soc.,* **112**, 677–691.

Betts, A. K., J.-L. Dufresne, H. L. Treut, J.-J. Morcrette, and C. Senior, 2004: On dynamic and thermodynamic components of cloud changes. *Climate Dyn.,* **22**, 71–86.

Bodas-Salcedo, A., M. J. Webb, S. Bony, H. Chepfer, J.-L. Dufresne, S. A. Klein, Y. Zhang, R. Marchandny, J. M. Haynes, R. Pincus, and V. O. John, 2011: COSP Satellite simulation software for model assessment. *Bull. Amer. Meteor. Soc.,* **92**, 1023–1043.

Collins, W. D., and Coauthors, 2006: The community climate system model version 3 (CCSM3). *J. Climate*, **19**, 2122–2143.

Dee, D. P., and Coauthors, 2011: The ERA-Interim reanalysis: configuraitiaon and performance of the data assimilation system. *Quart. J. Roy. Meteor. Soc.*, **137**, 553–597.

Del Genio, A. D., W. Kovari, M. –S. Yao, and J. Jonas, 2005: Cumulus microphysics and climate sensitivity. *J. Climate,* **18**, 2376–2387.

Delworth, T. L., and Coauthors, 2006: GFDL's CM2 global coupled climate models. Part 1: Formulation and simulation characteristics. *J. Climate,* **19**, 643–674.

Derbyshire, S. H., I Beau, P. Bechtold., J.-Y. Grandpeix, J.-M. Piriou, J.-L. Redelsperger, and P. M. M. Soares, 2004: Sensitivity of moist convection to environmental humidity. *Quart. J. Roy. Meteor. Soc.,* **130**, 3055–3079.

Emanuel, K. A., 1991: A scheme for representing cumulus convection in large-scale models. *J. Atmos. Sci.*, **48**, 2313–2329.

Emori, S., T. Nozawa, A. Numaguti, and I. Uno, 2001: Importance of cumulus parameterization for precipitation simulation over East Asia in June. *J. Meteor. Soc. Japan,* **79**, 939–947.

Fu, Q., and K. N. Liou, 1992: On the correlated *k*-distribution method for radiative transfer in nonhomogeneous atmospheres. *J. Atmos. Sci.,* **49,** 2139–2156.

Fu, Q., and K. N. Liou, 1993: Parameterization of the radiative properties of cirrus clouds. *J. Atmos. Sci.,* **50,** 2008–2025.

Grandpeix, J. Y., V. Phillips, and R. Tailleux, 2004: Improved mixing representation in Emanuel's convection scheme. *Quart. J. Roy. Meteor. Soc.,* **130**, 3207–3222.

Gregory, D., and M. J. Miller, 1989: A numerical study of the parameterization of deep tropical convection. *Quart. J. Roy. Meteor. Soc.,* **115**, 1209–1241.

Gregory, D., and P. R. Rowntree, 1990: A mass flux convection scheme with representation of cloud ensemble characteristics and stability-dependent closure. *Mon. Wea. Rev.,* **118**, 1483–1506.

Gregory, D., J.-J. Morcrette, C. Jakob, A. M. Beljaars, and T. Stockdale, 2000: Revision of convection, radiation, and cloud schemes in the ECMWF model. *Quart. J. Roy. Meteor. Soc.,* **126**, 1685–1710.

Hartmann, D. L., L. A. Moy, and Q. Fu, 2001: Tropical convection and the energy balance at the top of the atmosphere. *J. Climate,* **14**, 4495–4511.

Hourdin, F., and Coauthors, 2006: The LMDZ general circulation model: climate performance and sensitivity to parameterized physics with emphasis on tropical convection. *Climate Dyn.,* **27**, 787–813.

Ichikawa, H., H. Masunaga, and H. Kanzawa, 2009: Evaluation of precipitation and high-level cloud areas associated with large-scale circulation over the tropical Pacific in the CMIP3 models. *J. Meteor. Soc. Japan,* **87**, 771–789.

Ichikawa, H., H. Masunaga, Y. Tsushima, and H. Kanzawa, 2012: Reproducibility by climate models of cloud radiative forcing associated with tropical convection. *J. Climate,* **25,** 1247–1262.

K-1 Model Developers, 2004: K-1 coupled model (MIROC) description. H. Hasumi and S. Emori (eds.), K-1 technical report 1, Center for Climate System Research, University of Tokyo, 23 pp.

Kiehl, J. T., 1994: On the observed near cancellation between longwave and shortwave cloud forcing in tropical regions. *J. Climate*, **7**, 559–565.

Kiehl, J. T., and V. Ramanathan, 1990: Comparison of cloud forcing derived from the Earth Radiation Budget Experiment with that simulated by the NCAR Community Climate Model. *J. Geophys. Res.*, **95**,

11679–11698.

Klein, S. A., and C. Jakob, 1999: Varidation and sensitivities of frontal clouds simulated by the ECMWF model. *Mon. Wea. Rev.,* **127**, 2514–2531.

Kosaka, Y, H. Nakamura, M. Watanabe, and M. Kimoto, 2009: Analysis of the dynamics of a wave-like teleconnection pattern along the summertime Asian jet based on a reanalysis dataset and climate model simulations. *J. Meteor. Soc. Japan,* **87**, 561–580.

Kuber, T. L., D. L. Hartmann, and R. Wood, 2007: Radiative and convective driving of tropical high clouds. *J. Climate*, **20**, 5510–5527.

Kuo, H. L., 1965: On formation and intensification of tropical cyclones through latent heat release by cumulus convection. *J. Atmos. Sci.*, 22, 40–63.

Lin, J.-L, 2007: The double-ITCZ problem in IPCC AR4 coupled GCMs: ocean-atmosphere feedback analysis. *J. Climate,* **20**, 4497–4525.

Lin, J.-L, M.-I. Lee, D. Kim, I.-S. Kang, and D. M. W. Freirson, 2008: The impact of convective parameterization and moisture triggering on AGCM-simulated convectively coupled equatorial waves. *J. Climate,* **21**, 883–909.

Lin, W. Y., and M. H. Zhang, 2004: Evaluation of clouds and their rediative effects simulated by the NCAR community atmospheric model against satellite observations. *J. Climate,* **17**, 3302–3318.

Livesey, N. J., and Coauthors, 2011: Earth Observing System (EOS) Aura Microwave Limb Sounder (MLS) Version 3.3 Level 2 data quality and description document, Jet Propulsion Labratory.

Luo, Z, and W. B. Rossow, 2004: Characterizing tropical cirrus lifecycle, evolution, and interaction with upper-tropospheric water vapor using Lagrangian trajectory analysis of satellite observations. *J. Climate,* **17**, 4541–4563.

Mace, G. G., M. Deng, B. Soden, and E. Zipser, 2006: Association of tropical cirrus in the 10-15-km layer with deep convective sources: An observational study combining millimeter radar data and satellite-derived trajectories. *J. Atmos. Sci.,* **63**, 480–503.

Mace, G. G., S. Houser, S. Benson, S. A. Klein, and Q. Min, 2011: Critical evaluation of the ISCCP simulator using ground-based remote sensing data. *J. Climate,* **24**, 1598–1612.

Marchand, R. T., G. G. Mace, and T. P. Ackerman, 2008: Hydrometeor detection using CloudSat -an earth orbiting 94 GHz cloud radar. *J. Atmos. Oceanic. Technol,* **25**, 5190–533.

Martin, G. M., M. A. Ringer, V. D. Pope, A. Jones, C. Dearden, and T. J. Hinton, 2006: The physical properties of the atmosphere in the new Hadley Center Global Environmental Model (HadGEM1). Part I: model description and global climatology. *J. Climate,* **19**, 1274–1301.

Moorthi, S., and M. J. Suarez, 1992: Relaxed Arakawa-Schubert: A parameterization of moist convection for general circulation models. *Mon. Wea. Rev.*, **120**, 978–1002.

Nordeng, T. E., 1994: Extended versions of the convective parameterization scheme at ECMWF and their impact on the mean and transient activity of the model in the tropics. ECMWF Tech. Memo. 206, Reading, United Kingdom, 41pp.

Olsen, E.T., S. Granger, E. Manning, J. Blaisdell, 2007: AIRS/AMSU/HSB Version 5 Level 23 3 Quick Start, http://airs.jpl.nasa.gov/AskAirs.

Onogi, K., and Coauthors, 2007: The JRA-25 reanalysis. *J. Meteor. Soc. Japan*, **85**, 369–432.

Pan, D.-M., and D. A. Randall, 1998: A cumulus parameterization with a prognostic closure. *Quart. J. Roy. Meteor. Soc.*, **113**, 2108–2121.

Pope, V. D., M. L. Gallani, P. R. Rowntree, and R. A. Stratton, 2000: The impact of new physical parameterizations in the Hadley Centre climate model-HadAM3. *Climate Dyn.,* **16**, 123–146.

Ramanathan, V., R. D. Cess, E. F. Harrison, P. Minnis, B. R. Barkstrom, and D. L. Hartmann, 1989: Cloud-radiative forcing and climate: Results from the Earth Radiation Budget Experiment. *Science*, **243**, 57–63.

Rayner, N., A, D. E. Parker, E. B. Horton, C. K. Folland, L. V. Alexander, D. P. Rowell, E. C. Kent, and A. Kaplan, 2003: Global analysis of sea surface temperature, sea ice, and night marine air temperature since the late nineteenth century. *J. Geophys. Res.*, **108**, 4407 doi:10.1029/2002JD002670.

Ringer, M. A., and R. P. Allan, 2004: Evaluating climate model simulations of tropical cloud. *Tellus*, **56A**, 308–327.

Roeckner, E., and Coauthors, 2003: The atmospheric general circulation model ECHAM5. Part I: Model description. Max Planck Institute for Meteorology Rep. 349, 127 pp.

Rossow, W. B., and R. A. Schiffer, 1999: Advances in understanding clouds from ISCCP. *Bull. Amer. Meteor. Soc.,* **80**, 2261–2287.

Su, H., D. E. Waliser, J. H. Jiang, J.-L. Li, W. G. Read, J. W. Waters, and A. M. Tompkins, 2006: Relationship of upper tropospheric water vapor, clouds and SST: MLS observations, ECMWF analyses and GCM simulations. *Geophys. Res. Lett.,* **33**, L22802, doi:10.1029/2006GL027582.

Takayabu, Y. N., S. Shige, W.-K. Tao, and N. Hirota, 2010: Shallow and deep latent heating modes over tropical oceans observed with TRMM PR spectral latent heating data. *J. Climate*, **23**, 2030–2046.

Tiedtke, M., 1989: A comprehensive mass flux scheme for cumulus parameterization in large-scale models. *Mon. Wea. Rev.*, **117**, 1779–1800.

Tokioka, T., K. Yamazaki, A. Kitoh, and T. Ose, 1988: The equatorial 30-60 day oscillation and the Arakawa-Schubert penetrative cumulus parameterization. *J. Meteor. Soc. Japan,* **66**, 883–901.

Uppala, S. M., and Coauthors, 2005: The ERA-40 re-analysis. *Quart. J. Roy. Meteor. Soc.*, **131**, 2691–3012.

von Salzen, K., N. A. McFarlane, and M. Lazare, 2005: The role of shallow convection in the water and energy cycle of the atmosphere. *Climate Dyn.*, **25**, 671–688.

Waliser D. E., and Coauthors, 2009: Cloud ice: A climate model challenge with signs and expectations of progress. *J. Geophys. Res.,* **114**, D00A21, doi;10.1029/2008JD010015.

Webb, M., C. Senior, S. Bony, and J.-J. Morcrette, 2001: Combining ERBE and ISCCP data to assess clouds in the Hadley Centre, ECMWF, and LMD atmospheric models. *Climate Dyn.,* **17**, 905–922.

Webb, M., and Coauthors, 2006: On the contribution of local feedback mechanisms to the range of climate sensitivity in two GCM ensembles. *Climate Dyn.,* **27**, 17–38.

Williams, K. D., and G. Tselioudis, 2007: GCM intercomparison of global cloud regime: present-day evaluation and climate change response. *Climate Dyn,* **29**, 231–250.

Williams, K. D., and M. Webb, 2009: A quantitative performance assessment of cloud regimes in climate models. *Climate Dyn,* **33**, 141–157.

Wyant, M. C., C. S. Bretherton, J. T. Kiehl, I. M. Held, M. Z. Zhao, S. A. Klein, and B. J. Soden, 2006: A comparison of tropical cloud properties and responses in GCMs using mid-troposheric vertical velocity. *Climate Dyn.,* **27**, 261–279.

Yang, F., M. E. Schlesinger, and E. V. Rozanov, 2000: Description and performance of the UIUC 24-layer stratosphere-troposphere general-circulation model. *J. Geophys. Res.,* **105**, 17925–17954.

Yuan, J, D. L. Hartmann, and R. Wood, 2008: Dynamic effects on the tropical cloud radiative forcing and radiation budget. *J. Climate,* **21**, 2337–2351.

Zhang, M. H., and Coauthors, 2005: Comparing clouds and their seasonal variations in 10 atmospheric general circulation models with satellite measurements. *J. Geophys. Res.,* **110**, D15S02, doi:10.1029/2004jd005021.

Zhang, G. J., and N. A. McFarlane, 1995: Sensitivity of climate simulations to the parameterization of cumulus convection in the CCC-GCM. *Atmos.-Ocean,* **3**, 407–446.

Zhang, G. J., and M. Mu, 2005: Simulation of the Madden-Julian Oscillation in the NCAR CCSR3 using a revised Zhang-McFarlane convection parameterization scheme. *J. Climate,* **18**, 4046–4064.